



# Role of urban boundary layer dynamics and ventilation efficiency in a severe air pollution episode in Tehran, Iran

Forood Azargoshasbi<sup>1</sup> · Khosro Ashrafi<sup>1</sup> · Amir Houshang Ehsani<sup>1</sup>

Received: 16 May 2022 / Accepted: 15 May 2023 / Published online: 27 May 2023  
© The Author(s), under exclusive licence to Springer-Verlag GmbH Austria, part of Springer Nature 2023

## Abstract

Tehran faces a significant health challenge due to severe air pollution episodes during wintertime, which are associated with high concentrations of fine particulate matter with a diameter less than 2.5  $\mu\text{m}$  ( $\text{PM}_{2.5}$ ). In this study, we investigated meteorology conditions of one of the severe air pollution episodes, occurred from 27th December 2020 to 15th January 2021, using the Weather Research and Forecasting (WRF) model. To gain insights into this episode, we also modeled a clean episode for comparison. Model validation of land surface temperature using remote sensing showed acceptable performance as well as ground observations for other parameters. We then calculated the ventilation coefficient (VC) from the WRF outputs and analyzed the results statistically. Results indicate the severe reduction in both VC and planetary boundary layer height (PBLH) during the polluted episode. We further linked the decrease in PBLH and VC of the polluted episode to a high-pressure system above 1020 hPa. In contrast, the results for the clean episode indicate that the low-pressure system as low as 1010 hPa led to higher PBLH and VC than during the polluted episode. This low-pressure system favors the reduction of  $\text{PM}_{2.5}$  levels to lower than 21  $\mu\text{g m}^{-3}$ .

## 1 Introduction

Tehran is known to experience high concentrations of particulate matter, particularly during cold seasons. The polluted episodes have Air Quality Index (AQI) higher than the moderate range (Heger and Sarraf 2018; Ashrafi 2012; World Bank 2020; Yousefian et al. 2020). Particulate matters with a diameter less than 10  $\mu\text{m}$ , known as  $\text{PM}_{10}$ , can get deep into the lungs, and particle matters with a diameter less than 2.5  $\mu\text{m}$ , known as  $\text{PM}_{2.5}$ , can even get into the bloodstream that poses a greater risk to health than  $\text{PM}_{10}$  (EPA 2018). According to Heger and Sarraf (2018), Tehran is annually experiencing more than 4000 premature deaths from ambient  $\text{PM}_{2.5}$  air pollution and more than USD 2.6 billion economy costs associated with air pollutions, only considering the human health effect that underestimates the total economic costs from air pollution. Pishgar et al. (2020) have shown a dramatic increase in respiratory diseases from 2008 to 2018; and about 43,000 deaths due to respiratory diseases over the 10 years. Bayat et al. (2019) determined the

benefits associated with the decline of  $\text{PM}_{2.5}$  levels based on health targets and BenMAP-CE modeling. Their results indicate that economic benefits from reducing the annual concentration of  $\text{PM}_{2.5}$  to 10  $\mu\text{g m}^{-3}$  could be USD 1.9 billion.

Different types of emission sources and their link to the high concentrations of  $\text{PM}_{2.5}$  and  $\text{PM}_{10}$  have been identified by previous studies. Farahani and Arhami (2020) studied the contribution of local  $\text{PM}_{10}$  and  $\text{PM}_{2.5}$  sources and regional dust storms to the ambient air of Tehran using air pollution modeling. They found that the contribution of local emission sources as high as 75% and 82% of ambient  $\text{PM}_{10}$  and  $\text{PM}_{2.5}$  levels, respectively. Ashrafi et al. (2017) studied the potential of changes in radiation budgets by the high level of particulate matter (PM) from different  $\text{PM}_{10}$  sources of dust storms in Iran, using the WRF-Chem model. They found that dust aerosol led to short-wave radiation perturbation in both the earth's surface and top of the atmosphere. For instance, during one of the simulations, the domain-averaged short-wave radiation perturbation was  $-24.2 \text{ W m}^{-2}$ , and perturbations at the top of the atmosphere are lower than those on the surface and strongly dependent on surface albedo.

Based on the local emission inventory of Tehran, which is derived from major air pollution sources in Tehran, vehicle sources are known as the dominant source of  $\text{PM}_{2.5}$ , with a contribution of 85% among all sources (Shahbazi et al. 2016), due to their outdated technology

✉ Khosro Ashrafi  
khashrafi@ut.ac.ir

<sup>1</sup> Faculty of Environment, University of Tehran, 15 Ghods St, Enghelab Ave, Tehran 14155–6135, Iran

and abundance in the city (Heger and Sarraf 2018). However, Arhami et al. (2017) determined that re-suspended soil has a more significant contribution to the PM level of Tehran, using source apportionment method and chemical analysis of whole year measurement samples. They also showed the ratio of Dust/PM<sub>2.5</sub> was lower in the cold months than in the warm ones.

The health effects of PM<sub>2.5</sub> depend on its concentration that is highly controlled by emission sources and atmospheric conditions. Regardless of emission sources, the atmospheric parameters such as planetary boundary layer height (PBLH) and Ventilation Coefficient (VC) affect the concentration level of air pollutants in the ambient air significantly (Sujatha et al. 2016; Du et al. 2013). The atmospheric boundary layer controls the maximum mixing depth, corresponding with a more polluted region near-surface and relatively cleaner free atmosphere (Krishnan and Kunhikrishnan 2004). Mixing height alongside wind speed profile corresponding in VC, which is the power of pollution discharge or ventilation from captured air beyond the inversion layer (Cheremisinoff 2002). In this context, we refer to maximum mixing height as PBLH. Ashrafi et al. (2009) estimated PBLH and VC from 1998 to 2008 using sounding measurements during different seasons for Tehran. They reported that PBLH shows the lowest values during December and January. They measured VC to be about 5000 m<sup>2</sup>s<sup>-1</sup>, due to the low PBLH values, which has the lowest value compared to other months. (Ashrafi et al. 2009). These studies are limited, and the dynamics and particularly the spatial patterns of PBLH and VC are, to the most part, unknown in the city.

Furthermore, the impact of heat mitigation measures on the PBLH and air quality has been examined by previous studies (Arghavani et al. 2019; Vahmani et al. 2016). It is reported that although heat mitigation strategies such as cool and green roofs highly affect the heat budget and are suitable for reducing the ambient temperature, they can have a negative effect on severe air pollution episodes due to the reduction of PBLH and change of wind flow patterns (Epstein et al. 2017; Arghavani et al. 2019).

Although the government applied restriction on the nighttime traffic from 2020 November due to control on the spread of COVID-19, which could reduce emission from mobile sources, the concentration of pollutants in the city was elevated with respect to past years. Su et al. (2020) also linked this abnormal high PM level during lockdowns in northern China to low PBLH. It could be concluded that low PBLH and VC probably play a significant role in the air pollution levels of Tehran, whereas some emission control could not even have an effect. This is important to understand since lockdowns have reduced air pollution levels in other cities (He et al. 2020).

The formation and dynamics of PBLH and VC in Tehran are not well understood although they were measured by Ashrafi et al. (2009). This study aims to address this knowledge gap by investigating the roles of dynamic PBLH and VC in a severe air pollution episode that occurred in the winter of 2021. To investigate these roles in the air pollution of Tehran, in this study, we used the WRF model to investigate the role of dynamic PBLH and VC in the severe air pollution episode of winter 2021. To do this, first, we set up the model for the Tehran boundary. Then we model the PBLH and VC for the study period using the WRF model outputs. We examined the model performance using meteorology datasets and satellite surface temperature products. To understand the relation of PBLH and VC to PM<sub>2.5</sub> levels, we extract PM<sub>2.5</sub> concentrations from available air pollution measurement stations. Then we looked for the possible cause of changes in PBLH and VC that might have led to high levels of PM<sub>2.5</sub> in the study period.

## 2 Materials and methods

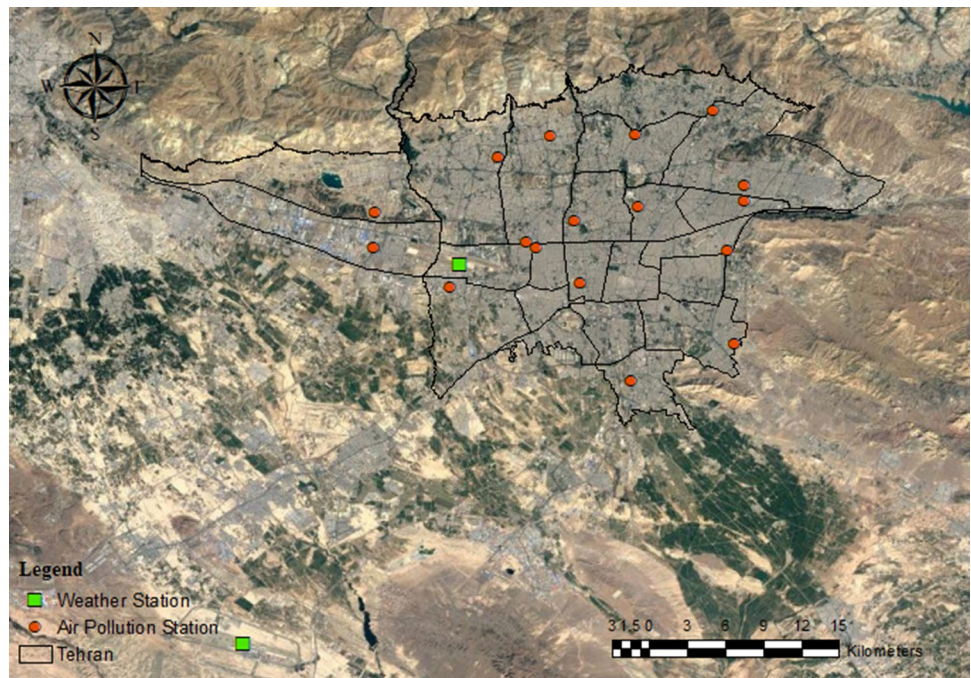
### 2.1 Study domain

Tehran, the capital of Iran, faces the Alborz Mountain in the north and flat plains of agricultural lands in the south (Fig. 1). According to the 2016 census, the population of the city is 8,737,510 people (Statistical Center of Iran 2016). The average annual temperature is 19.1 °C, and the average minimum and maximum temperatures are 14.2 °C and 36 °C, respectively. Also, the average rainfall of this city is 209.3 mm (Statistical Center of Iran 2021).

### 2.2 Polluted and clean episode

Severe high air pollution of PM<sub>2.5</sub> happened from 30th December 2020 to 15th January 2021, which in fourteen days, Air Quality Index (AQI) exceeded 150 (unhealthy according to EPA (EPA 2021)). Such a long-lasting highly polluted episode has not happened from 2014 to 2021. According to ground measurements in the study period in all stations (Fig. 1), the maximum hourly means of PM<sub>10</sub> and PM<sub>2.5</sub> reached approximately 170 µgm<sup>-3</sup>, and 100 µgm<sup>-3</sup>, respectively (Fig. 2a). Therefore, we selected the period of 27th December 2020 to 15th January 2021 as the polluted episode. We choose this time to determine the role of PBLH and VC in these high PM<sub>2.5</sub> level episodes. To assess PBLH and VC roles in clean days, we select 17th January 2021 to 23rd January 2021 as the clean episode.

**Fig. 1** The study area map. Red circles show locations of 17 air pollution measurement stations within the Tehran boundary. Green squares show locations of two synoptic stations, Mehrabad within the Tehran boundary and Imam-Khomeini outside of the city (Google Earth)



### 2.3 Model configuration

In this study, we used the state-of-the-art Weather Research and Forecasting (WRF) version 4.3, the non-hydrostatic, an Eulerian Mesoscale NWP model, capable of using different physic parameterization (Skamarock et al. 2019; Wang et al. 2018), to simulate the atmosphere condition and weather parameters for Tehran domain. WRF is coupled to an urban canopy model alongside the land surface model that resolves urban canopy processes and surface energy balance accounting for the nature of urban surfaces (Chen et al. 2011).

We used three nested domains to calculate the urban meteorology parameters of Tehran, as shown in Fig. 3a. The first (d01), second (d02), and third (d03) domains consisted of  $90 \times 70$ ,  $64 \times 52$ , and  $46 \times 46$  grid cells and grid resolution of 18, 6, and 2 km, respectively. We used the 6 h FNL datasets of the National Center of Environmental Prediction (NCEP), with the resolution of  $0.5^\circ$  for boundary and initial conditions of the WRF model.

The physic parameterization schemes used in this study were the Lin scheme (Janjić 1994) for microphysics, the Kain-Fritsch scheme (Kain 2004) for cumulus parameterization, the Rapid Radiative Transfer Model (RRTM) scheme (Mlawer et al. 1997) for long-wave radiation, the Goddard scheme (Chou and Suarez 1999) for short-wave radiation, the MYJ scheme (Chen and Sun 2002) for the planetary boundary layer, and the atmosphere model is coupled to the Noah land surface model (Niu et al. 2011) including single-layer urban canopy model (Kusaka and

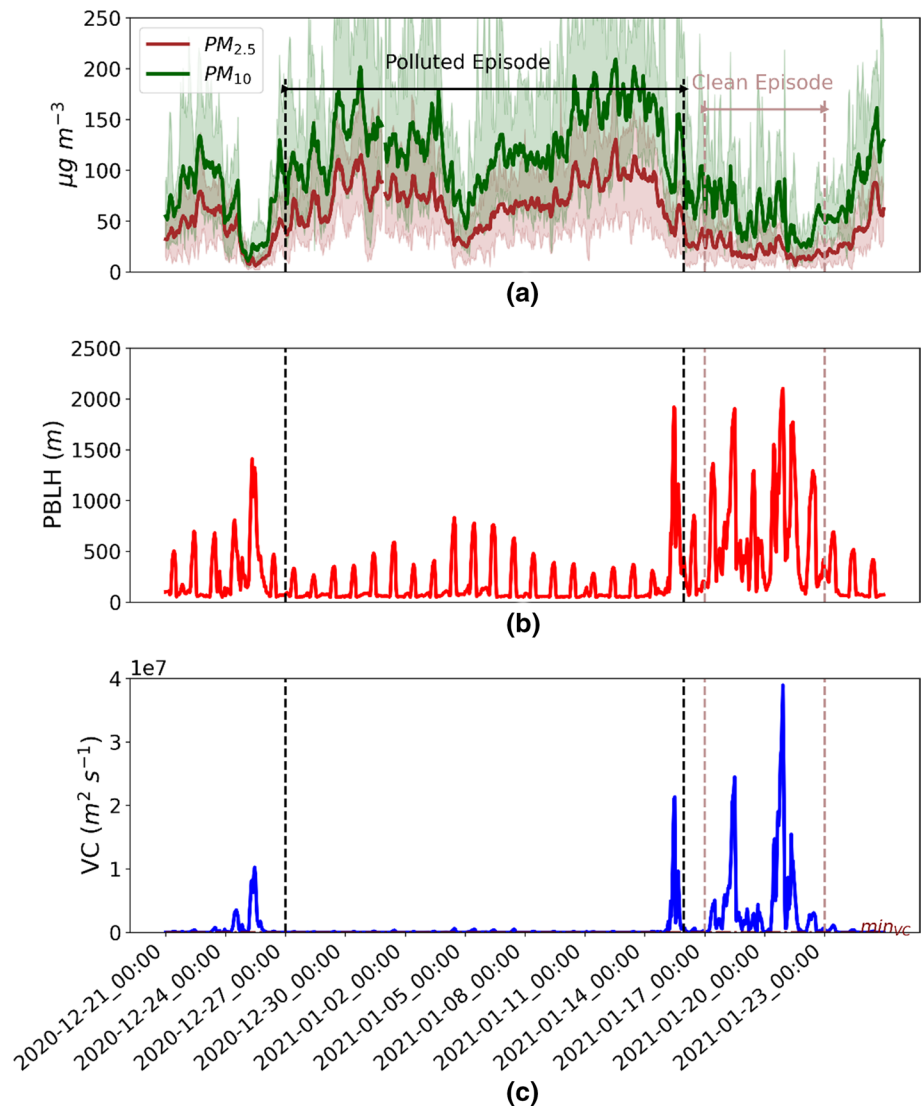
Kimura 2004). For regions outside of the United States of America, the default land-use and urban fraction are inaccurate and have missing values. Therefore, we extract land use categories, urban fraction (FRC\_URB), and types (Demuzere et al. 2021) based on the local climate zone (LCZ) classes dataset (Izadi 2021), as shown in Fig. 3b. These extracted parameters were used as terrestrial data input. We also used urban parameters as shown in Table 1, proposed by Arghavani et al. 2019, in the urban parameter table (URBPARAM.TBL). Based on the extracted urban types, we updated both land use index and green fraction for both January and December according to the LCZ dataset, as shown in Figs. 4 and 5, respectively.

Furthermore, we developed a method to define land use fraction for three urban types according to LCZ classes, as shown in Fig. 4. It must be remarked that for two outer domains, 21 modified MODIS land use cover classes dataset was used in all simulations. Twelve hours were discarded for the spin-up of modeling. Model configurations are summarized in Table 2. To have a more accurate prediction of meteorology conditions, we separated the length of the study period and ran the model every three days. The purpose of the developed methodology is to have a better land surface temperature and meteorology representation compared to the default method.

Although the latest version of the WRF model, WRF 4.3, introduced a new feature called WRF-BEP that allows for the use of Building Energy Parametrization with Local Climate Zone (LCZ) input data, we opted to use WRF coupled



**Fig. 2** Time series of **a**  $PM_{10}$  and  $PM_{2.5}$  concentrations from stationary measurements with errors (maximums and minimums), **b** PBLH, and **c** VC from the WRF model within Tehran boundaries throughout the study period



to single layer Urban Canopy Model (WRF-UCM) due to a lack of detailed information on the city’s buildings. We performed all simulations with the modified land use type, land use fraction, and green fraction (as presented in Figs. 4 and 5). However, there were some uncertainties in urban parameterization, as we discussed later in the Discussion chapter.

**2.4 Calculation of PBLH and VC**

PBLH is simulated by WRF-UCM over the city (domain d03). Then, we used PBLH to calculate the VC using the integration of wind speed across the PBLH. Since the wind speed profile is needed to be calculated in the PBLH using the WRF outputs, we interpolated the wind speed in the PBLH. Then we calculated the VC using Eq. (1),

$$\begin{aligned}
 VC(x, y) &= \sum_1^{PBLH} f(wind_i, z_i) \\
 &= \begin{cases} z_i^2 wind_i & i = 1 \\ \frac{(wind_i z_i + wind_{i-1} z_{i-1})(z_i - z_{i-1})}{2} & 1 < i < PBLH \\ \frac{(wind_{PBL} z_{PBL} + wind_{i-1} z_{i-1})(z_{PBL} - z_{i-1})}{2} & i = PBLH \end{cases} \quad (1)
 \end{aligned}$$

where  $VC(x, y)$  is the VC at each cell of the study domain at a time,  $i$  is the model’s layer number from ground,  $z_i$  presents the model’s layer height,  $wind_i$  presents the model’s layer horizontal wind speed (calculated from  $\sqrt{u_i^2 + v_i^2}$ ),  $wind_{PBL}$  and  $z_{PBL}$  are wind speed at PBLH from previous step, and height of PBLH, respectively.

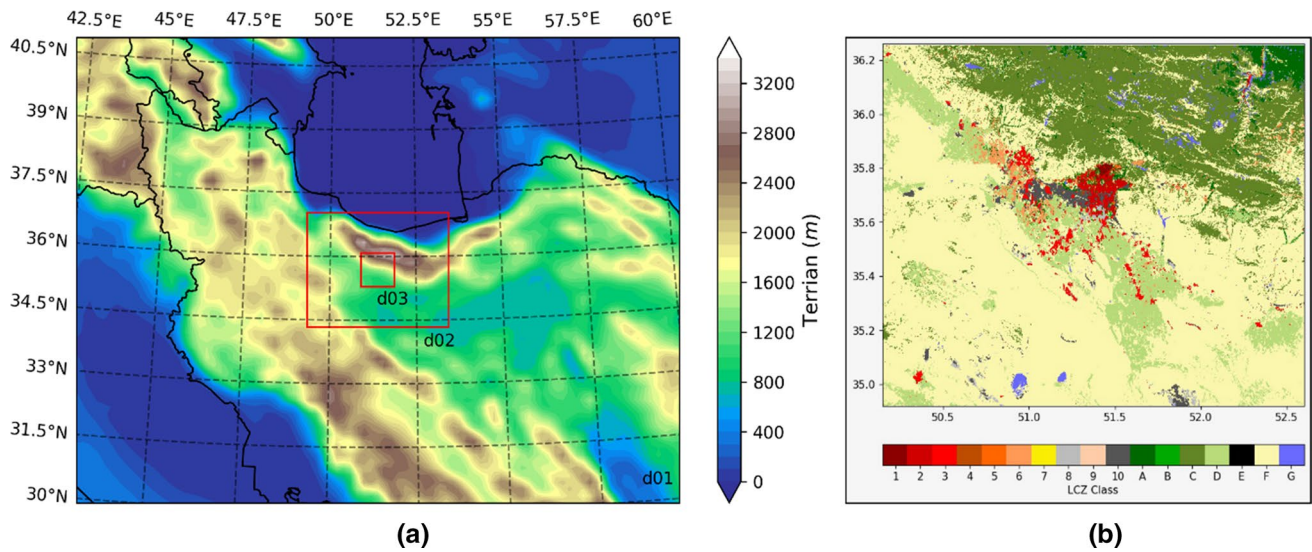


**Fig. 3** **a** Topography of three nested domains in WRF modeling. **b** The local climate zone classes dataset (Izadi 2021) is used to generate urban categories

### 2.5 Statistical analysis method

To perform statistical analysis of the model performance, we used Pearson correlation coefficient ( $R$ ), root means squared error (RMSE), and mean absolute error (MAE) using Eqs. (2, 3, 4) and, respectively.

$$R = \frac{\text{cov}(P, O)}{\sigma_P \sigma_O} \tag{2}$$

$$\text{RMSE} = \sqrt{\frac{1}{n} \sum_{i=1}^n (P_i - O_i)^2} \tag{3}$$

$$\text{MAE} = \frac{1}{n} \sum_{i=1}^n |P_i - O_i| \tag{4}$$

where  $P$  and  $O$  are predictions and observations, respectively,  $\text{cov}$  is the covariance function,  $\sigma_P$  and  $\sigma_O$  are standard deviations of predicted and observed samples, respectively, and  $n$  is the number of samples.

### 2.6 Meteorological and pollutants dataset

We obtained the hourly measurements of meteorological parameters, relative humidity at 2 m ( $\text{RH}_2$ ), wind speed at 10 m ( $\text{WIND}_{10}$ ), and temperature at 2 m ( $T_2$ ), for use in model validation from the ASOS Network of IOWA

**Table 1** Single layer urban canopy model parameters (Arghavani et al. 2019)

	Low residential	High residential	Commercial/industrial
FRC_URB—fraction (modified)	0.5	0.9 ( <b>0.75</b> )	0.95 ( <b>0.85</b> )
Roof level (building height) [m]	5.0	7.0	10.0
Anthropogenic heat [ $\text{W m}^{-2}$ ]	20.0	50.0	90.0
Anthropogenic latent heat [ $\text{W m}^{-2}$ ]	20.0	25.0	40.0
Surface albedo of roof	0.2	0.2	0.2
IRI_SCHEME** = 1			
DDZR*** (4 layers): 0.05, 0.05, 0.05, 0.05			
DZGR****: (1) Top soil layer=0.05 (2) Soil layer=0.1 (3) Growing medium layer=0.15 (4) concrete roof=0.2 [m]			

Normal font shows default model’s configuration values, and bold font shows modified configuration values

\*\*Urban irrigation scheme for vegetation in the urban area and green roof

\*\*\*Thickness of each roof layer

\*\*\*\*Thickness of each layer on the green roof

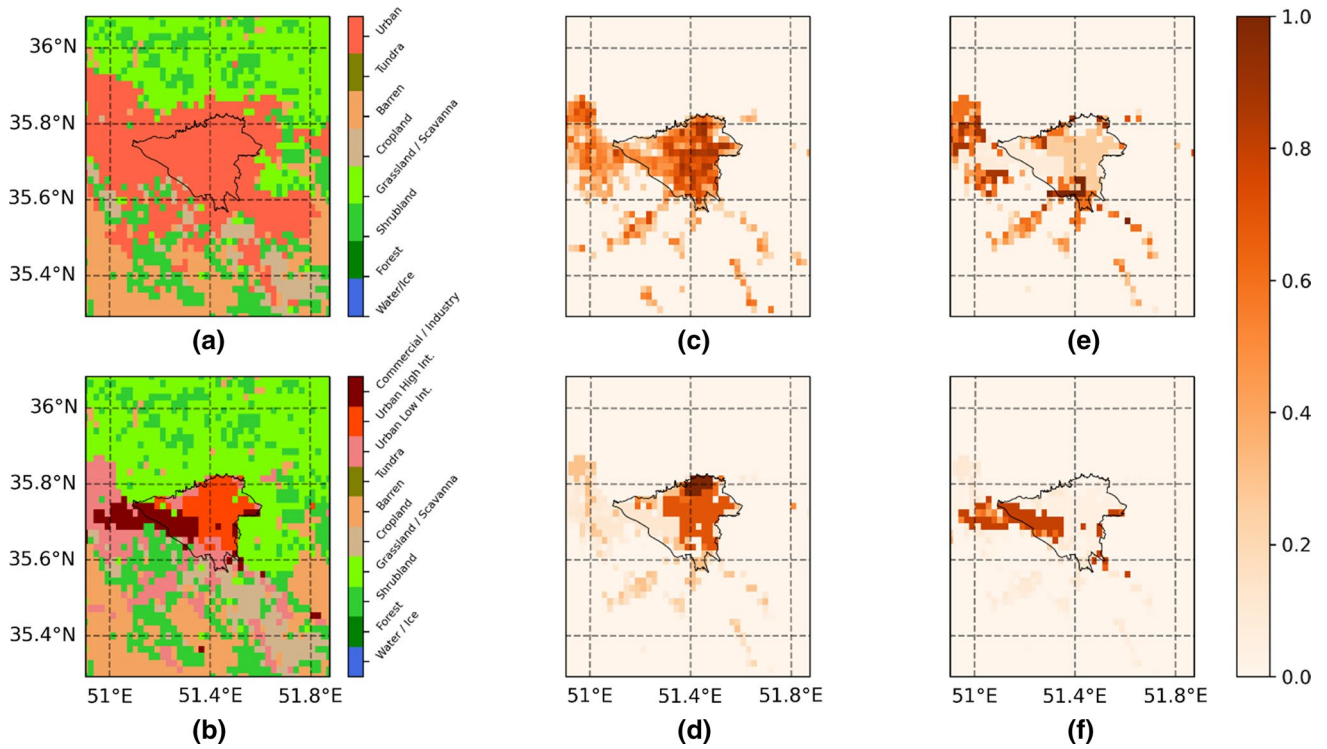


**Fig. 4** (Left column) Land use index (top) default, and (bottom) updated. (Top center) urban fraction. (Bottom center) land use fraction for high residential urban type. (Top right) land use fraction for low residential urban type. (Bottom right) land use fraction for commercial/industry urban type

**Fig. 5** Green fraction of default (left column) and updated (right column) in all simulations in January (bottom row) and December (top row)

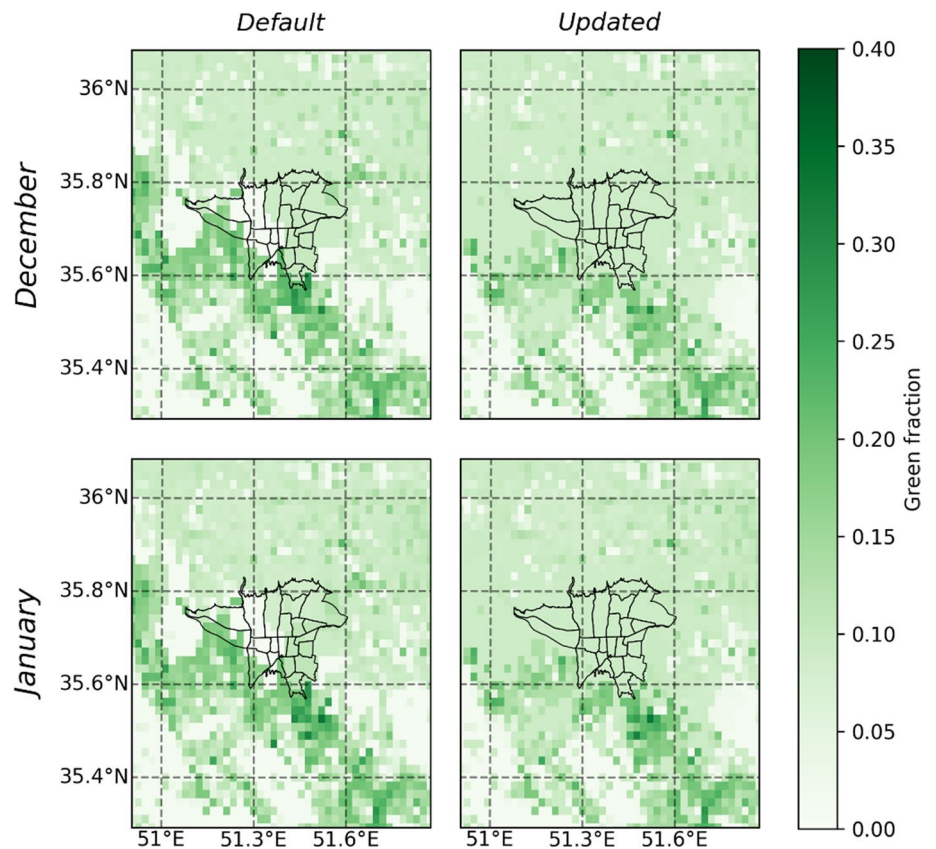




**Table 2** Model configuration summary

Periods	2020-12-20_12:00 to 2021-01-26_00:00 (37 days)
Microphysics	Lin
Radiation	Short-wave: Goddard Long-wave: RRTM
Planetary boundary layer	MYJ
Surface layer	Noah
Urban physics	Single-layer Urban Canopy
Cumulus parameterization	Kain- Fritsch
Horizontal spacing	d01: 18 km (90×70 points) d02: 6 km (64×52 points) d03: 2 km (46×46 points)
Time step	d01: 108 s, d02: 36 s, d03: 12 s
BC & IC	FNLs (0.5° every 6 h)
Spin-up	12 h

State University, which is available online through their website (Iowa Environmental Mesonet 2021). The ground observations were obtained for two available synoptic stations in d03 of modeling, Mehrabad and Imam-Khomeini airports, with station codes of OIII and OIIE, respectively. Mehrabad station is located at 51°18'12.96" east and 35°41'8.52" north, inside the city. Imam-Khomeini station is located at 51°8'60.00" east and 35°25'0.12" north, outside the city (as shown in Fig. 1 with green square). Mehrabad and Imam-Khomeini stations were chosen due to their representation of the urban and rural areas of d03, respectively.

We obtained hourly mean air pollutants ( $PM_{10}$  and  $PM_{2.5}$ ) measurements through the Tehran Air Quality Control

Company (AQCC) online website, which has an archive of available records. We extracted and averaged  $PM_{10}$  and  $PM_{2.5}$  measured for all available stations (seventeen stations shown in Fig. 1 with red circles) in Tehran for each hour of the modeling period (AQCC 2021). Then, we averaged all parameters for each day to better judge the impact of PBLH and VC on the concentrations.

Furthermore, we used land surface temperature products from MODIS onboard Terra and Aqua (MOD11\_L2.v006) to evaluate the model performance in the second and third domains. Also, we used Wyoming university upper air dataset for the Mehrabad Station to evaluate the model performance vertically.

## 2.7 Understanding the causes of PBLH and VC fluctuations

In Causality of PBLH and VC fluctuations, we extracted different parameters, such as sensible heat flux (HFX), latent heat flux (LH),  $T_2$ , first layer cloud fraction (CF), and sea level pressure (SLP), from the WRF model and mapped over d03 within the Tehran boundaries. We did so to have a better understanding of the causality of these changes in PBLH and VC. We also calculated the daily average of these parameters within the Tehran boundaries from the model. Moreover, we looked for the formation of high- and low-pressure systems in the first domain at 500 millibar level. We mapped the PMs spatial distribution during the study period, the clean and polluted episodes in the city. Finally, we performed statistical analysis of mean, standard deviation (std), first, second, and third quartile ( $Q_1$ ,  $Q_2$ , and  $Q_3$ , respectively) on the extracted parameters and pollutions.

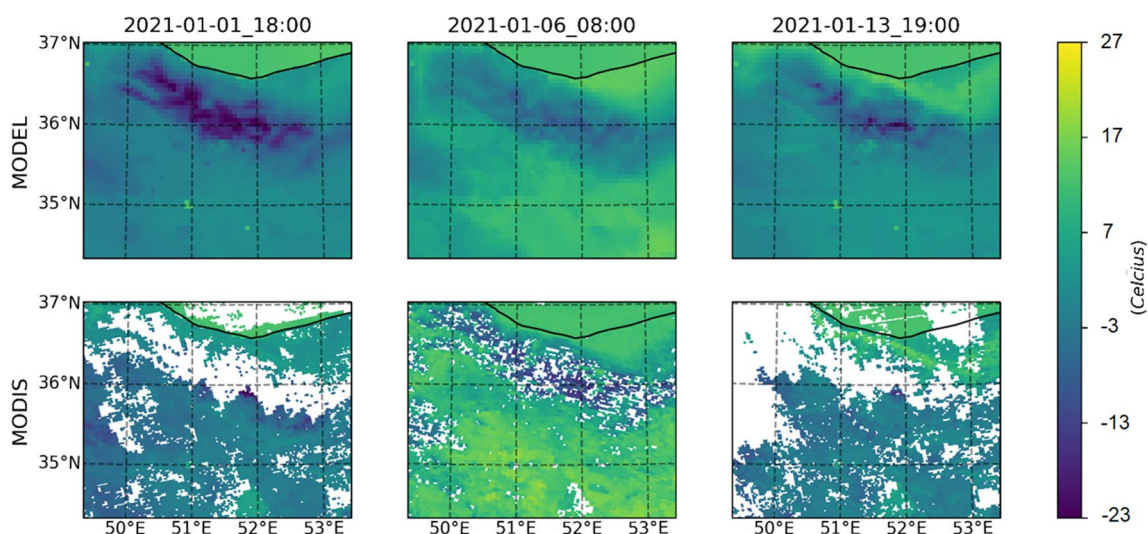


**Fig. 6** Land surface temperature of the second domain. (top row) the WRF model, (bottom row) the MODIS product (MOD11\_L2.v006). The corresponding times to the columns are (left column) 2021-01-01

18:00, (middle column) 2021-01-06 08:00, and (right column) 2021-01-13 19:00

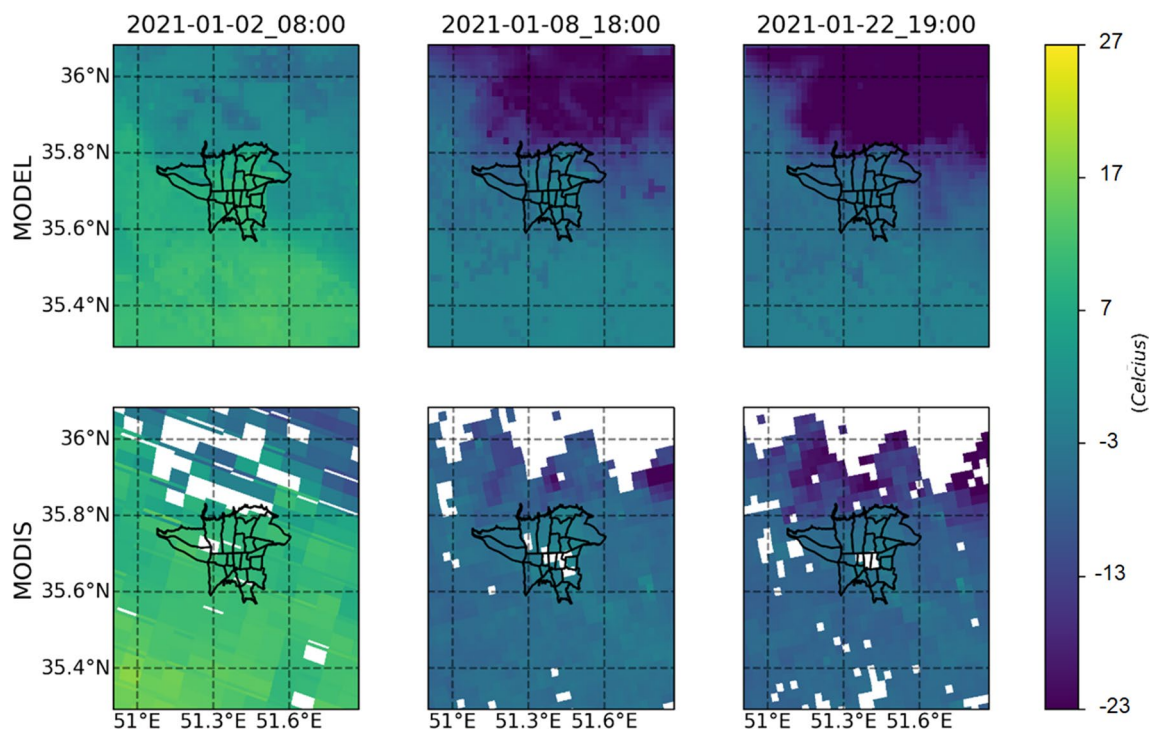


**Fig. 7** Land surface temperature of the third domain. (top row) the WRF model, (bottom row) the MODIS product (MOD11\_L2.v006). The corresponding times to the columns are (left column) 2021-01-02 08:00, (middle column) 2021-01-08 18:00, and (right column) 2021-01-22 19:00

### 3 Results

#### 3.1 Model validation

We validated the modified model with three different methods. First, we used  $RH_2$ ,  $WIND_{10}$ , and  $T_2$  parameters of two synoptic stations of Mehrabad and Imam-Khomeini airports to validate the WRF model in the study period. Then, we used land surface temperature to evaluate the performance of the model for both the second (Fig. 6) and third domain (Fig. 7). Afterall, we used temperature, wind speed, potential temperature Wyoming dataset for the Mehrabad station to evaluate the vertical performance of the model (Fig. 8).

We observed an acceptable performance of hourly variation of mentioned parameters over the Tehran modeling domain from the WRF model on both stations, as shown in Fig. 9 for time series plots and Fig. 10 for model performance and its accuracy correlations. In Table 3, we presented the statistical analysis of the model.

Although the model could capture all three parameters patterns in the Imam-Khomeini station with acceptable performance (Figs. 9 and 10), the model underestimates the 2 m temperature at Mehrabad station (mainly during the nights). The model could not capture the RH in the Mehrabad station; since RH correlates to the temperature, this could explain the model performance in the Mehrabad station for RH. The wind speed MSE at the Mehrabad

station was measured to be  $2.4 \text{ ms}^{-1}$ . However, it is important to note that this measurement may contain some errors that could be attributed to the method of wind speed measurement utilized at the station. Specifically, wind speeds are reported as rounded numbers, and any wind speeds below  $2 \text{ ms}^{-1}$  are recorded as 0. These factors may contribute to the observed errors in the wind speed measurement at the station. We looked through the vertical profile of the Mehrabad station (Fig. 8) for the development of temperature profile in the urban area. The model could capture all available parameters vertical profile well for the duration of the modeling. We associated this underestimation in the 2 m temperature with land use type (which is in this case the urban type) that is discussed in details by Molnár et al. (2019). Unfortunately, other weather stations were not accessible to the authors for comparison.

The model could capture land surface temperature in the second (Fig. 6) and third (Fig. 7) domains when we set up the model with the modified green fraction and land use type (figures are not shown). Vahmani and Ban-Weiss (2016) also showed modified remote sensing green fraction yield better performance than the model's default. While the model could capture the spatial pattern and variation during the modeling period, sometimes the model could not capture the minimum temperature well, mainly in the high elevation of the Alborz mountains (figures are not shown).



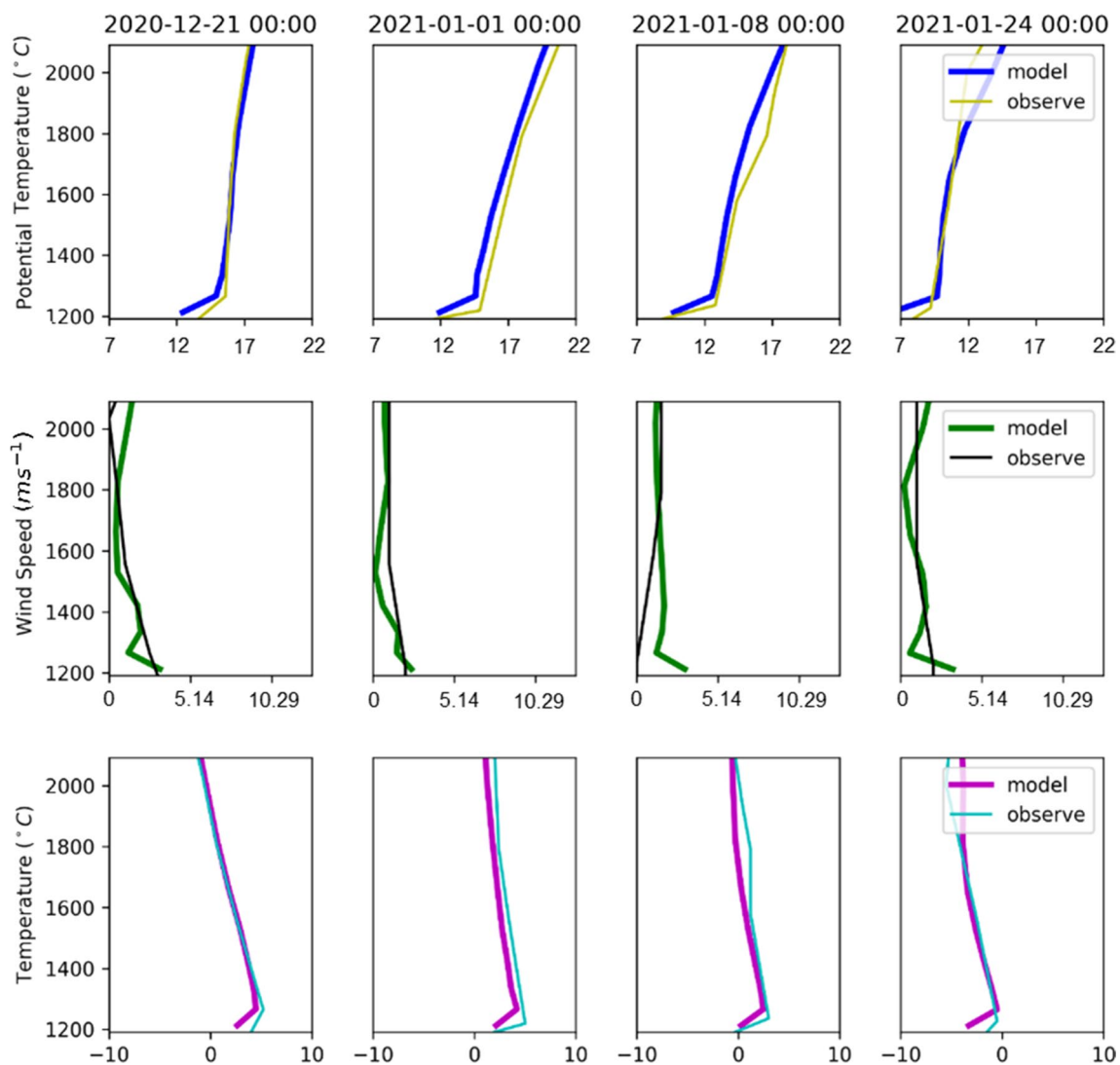


**Fig. 8** Vertical evaluation of the model for the potential temperature (top row), wind speed (middle row), and temperature (bottom row) parameters. From left the time steps are 2020-12-21 00:00, 2021-01-01 00:00, 2021-01-08 00:00, 2021-01-24 00:00. the y-axes are the height in meters

### 3.2 Impact of VC and PBLH on PM levels

To assess the impact of VC and PBLH on PM levels, we used only cells within the Tehran boundaries (Fig. 4) to calculate the average PBLH and VC of the city. Also, we averaged  $PM_{2.5}$  and  $PM_{10}$  concentrations for all seventeen stations, as shown in Fig. 1, to correlate the PM levels with PBLH and VC, as shown in Fig. 2.

$PM_{2.5}$  and  $PM_{10}$  levels, averaged over all stations, reached higher levels during the period of the polluted episode than the period of the clean one, as shown in Fig. 2a. During the polluted episode, maximum and minimum  $PM_{2.5}$  reached 130.4 and 24.7  $\mu g m^{-3}$ , respectively. In the clean episode, the maximum and minimum were 40.9 and 4.6  $\mu g m^{-3}$ , respectively. Differences between  $PM_{10}$  and  $PM_{2.5}$  in the polluted episode period were higher than in the clean episode

one, with the mean of 56.5 and 33.6  $\mu g m^{-3}$ , respectively. The maximum average  $PM_{10}$  concentration in the polluted reached 209.3  $\mu g m^{-3}$ . Table 4 shows other statistical analyses of the polluted and the clean episode and how the PMs are distributed during both episodes. Also, we mapped the spatial pattern of  $PM_{2.5}$  and  $PM_{10}$  and their ratio ( $PM_{2.5}/PM_{10}$ ) over Tehran (as shown in Fig. 11).  $PM_{10}$  was the dominant pollutant in the southwest of Tehran in the clean and polluted episodes, while  $PM_{2.5}$  was the dominant pollutant in the inner and north of the city (Fig. 11).

Boundary layer dynamics and wind strength govern the concentration of the pollutants at any given location. Hence, VC plays a significant role in the dispersion of pollutants (Iyer and Raj 2013; Mahalakshmi et al. 2011). Over the simulated 37 days, PBLH in the period of the polluted episode was significantly lower than in the clean episode, as shown

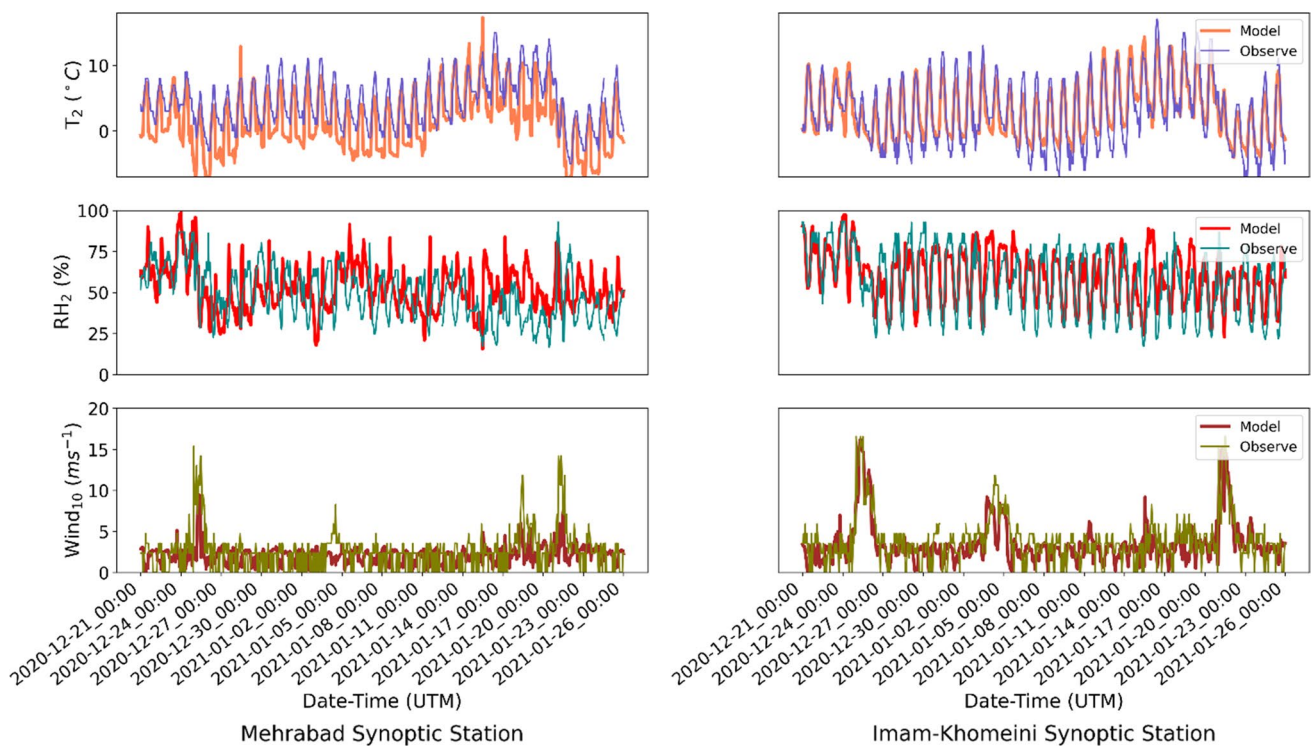


**Fig. 9** Times series plots of model performance and stationary measurements for the period of 2020-12-21\_00:00 to 2021-01-26\_00:00, top row temperature at 2 m, middle row relative humidity at 2 m, bot-

tom row wind speed at 10 m, left column Mehrabad station, and right column Imam-Khomeini station

in Fig. 2b. As a result of the decrease in PBLH alongside low dominant wind speed, a huge decline in VC occurred in the polluted episode (Fig. 2c). When VC dropped under  $0.7 \times 10^5 \text{ m}^2\text{s}^{-1}$  in the period of the polluted episode, the accumulation of both  $\text{PM}_{2.5}$  and  $\text{PM}_{10}$  occurred. In the middle of the polluted episode, a slight increase in PBLH and VC occurred, leading to a decrease in PM levels. We further linked this increase in the middle of the polluted episode to the presence of the low-pressure system.

The average VC above  $4.7 \times 10^6 \text{ m}^2\text{s}^{-1}$  favored effective dispersion and reduction of  $\text{PM}_{2.5}$  and  $\text{PM}_{10}$  levels in the period of the clean episode (Fig. 2). On the other hand, the

high VC and PBLH during the clean episode show a significant correlation with the drop in both  $\text{PM}_{10}$  and  $\text{PM}_{2.5}$  levels. The low VC and PBLH in the polluted episode show a significant correlation with the  $\text{PM}_{2.5}$  and  $\text{PM}_{10}$  accumulation in the city. As shown in Fig. 2, an average PBLH of less than 1000 m correlates with an average VC of less than  $1 \times 10^5 \text{ m}^2\text{s}^{-1}$ . Also, the average PBLH higher than 1000 m correlates with the average VC higher than  $2 \times 10^6 \text{ m}^2\text{s}^{-1}$ . We showed the statistical analysis of PBLH and VC in Table 4.

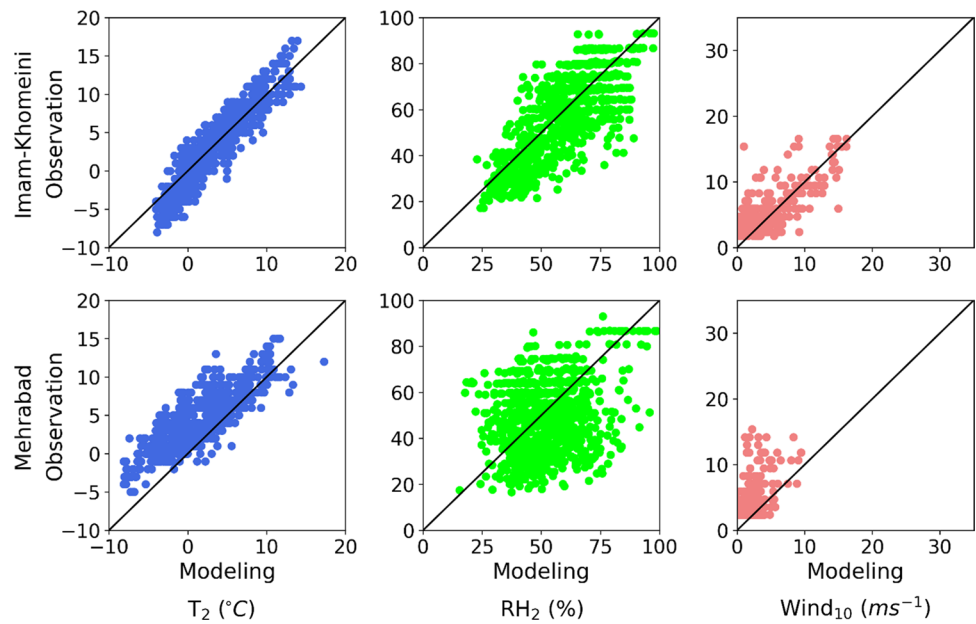
### 3.3 Causality of PBLH and VC fluctuations

We, in Fig. 12, depict the daily average of different meteorology parameters that might affect the PBLH and VC in the period of study. Differences between daily  $\text{PM}_{10}$  and  $\text{PM}_{2.5}$  increased significantly during the polluted episode, while during the clean episode, these differences were at their minimum (Fig. 12a). The spatial pattern of  $\text{PM}_{2.5}/\text{PM}_{10}$  (PM ratio) in the city (Fig. 11) illustrates that during the polluted episode, inner-city  $\text{PM}_{2.5}$  had high pollution portion. Also, the west and south side of the city had a higher PM ratio than the north and east side. Figure 12 illustrates our findings regarding the influence of wind speed on the formation of VC and its impact on pollutant dispersion. Specifically, we observed that during the clean episode, when wind speeds

**Table 3** Statistical analysis of model

Parameters	Station	R	RMSE	MAE
Mehrabad				
RH		0.43	18.7 (%)	15.4 (%)
Temperature		0.86	3.7 (°C)	3.1 (°C)
Wind Speed		0.62	2.4 ( $\text{ms}^{-1}$ )	1.8 ( $\text{ms}^{-1}$ )
Imam-Khomeini				
RH		0.78	12.4 (%)	10.1 (%)
Temperature		0.93	1.9 (°C)	1.6 (°C)
Wind Speed		0.71	2.1 ( $\text{ms}^{-1}$ )	1.6 ( $\text{ms}^{-1}$ )

**Fig. 10** Model performance and correlations of modeling versus Observations, top row Imam-Khomeini synoptic station, bottom row Mehrabad synoptic station, left column Temperature at 2 m, middle column relative humidity at 2 m, and right column wind speed at 10 m for the period of study



were notably higher, VC played a more significant role in facilitating the dispersion of pollutants. This highlights the importance of considering wind speed as a key factor in understanding the dynamics of air pollution and the role of various compounds in this process.

At the beginning of the polluted episode, the daily average PM levels rose. In the middle of the polluted episode, two drops in PM levels resulted in a decrease in PM levels. There was a decline in PM levels for two days at the late

polluted episode despite increasing VC (Fig. 12a, b). This pollution is due to the time that wind needs to transport and disperse accumulated pollutants. Also, prior to the polluted episode, although VC dropped significantly, one day of accumulation of pollutants was required to increase the city’s pollutants to the unhealthy range (2020–12–26). Since sensible heat flux, latent heat flux, cloud fraction, temperature, and sea level pressure play essential roles in the formation

**Table 4** Parameters description of mean, std, min,  $Q_1$ ,  $Q_2$ ,  $Q_3$ , and max for  $\text{PM}_{2.5}$ ,  $\text{PM}_{10}$ , PBLH, VC, sensible heat flux, latent heat flux, air temperature, cloud fraction, and sea level pressure for the polluted and clean episodes

	Parameter	Mean	Std	Min	$Q_1$	$Q_2$	$Q_3$	Max
The polluted episode	PBLH (m)	167.7	221.8	47.1	55.7	70.4	197.1	1918.1
	VC ( $\text{m}^2\text{s}^{-1}$ )	$0.3 \times 10^6$	$1.7 \times 10^6$	$7.6 \times 10^2$	$3.3 \times 10^3$	$7.4 \times 10^3$	$5.0 \times 10^4$	$2.1 \times 10^7$
	HFX ( $\text{Wm}^{-2}$ )	2.3	33.3	-38.7	-20.6	-12.6	15.3	110.4
	CF (%)	0	10	0	0	0	0	80
	$T_2$ ( $^{\circ}\text{C}$ )	2.0	3.6	-4.0	v1.0	1.5	4.6	12.8
	SLP (hPa)	1024.8	3.9	1013.2	1023.4	1025.2	1027.1	1031.1
	LH ( $\text{Wm}^{-2}$ )	23.5	37.2	-2.4	-0.6	0.3	48.7	137.9
	$\text{PM}_{2.5}$ ( $\mu\text{gm}^{-3}$ )	71.9	21.6	24.7	57.8	70.5	89.5	130.4
	$\text{PM}_{10}$ ( $\mu\text{gm}^{-3}$ )	128.4	33.8	42.7	105.2	126.0	153.3	209.3
	The clean episode	PBLH (m)	699.8	523.0	79.7	271.5	518.0	1072.3
VC ( $\text{m}^2\text{s}^{-1}$ )		$4.7 \times 10^6$	$7.2 \times 10^6$	$9.6 \times 10^4$	$0.5 \times 10^6$	$2.0 \times 10^6$	$4.8 \times 10^6$	$3.9 \times 10^7$
HFX ( $\text{Wm}^{-2}$ )		6.7	52.1	-49.7	-28.8	-16.1	36.5	165.3
CF (%)		20	20	0	0	0	30	100
$T_2$ ( $^{\circ}\text{C}$ )		2.5	4.5	-6.7	0.6	3.3	4.6	9.2
SLP (hPa)		1018.8	7.7	1008.3	1012.9	1016.9	1020.1	1034.6
LH ( $\text{Wm}^{-2}$ )		33.9	42.0	-0.5	3.1	10.0	64.2	140.2
$\text{PM}_{2.5}$ ( $\mu\text{gm}^{-3}$ )		11.5	6.9	0.0	5.8	11.5	17.3	23.0
$\text{PM}_{10}$ ( $\mu\text{gm}^{-3}$ )		21.0	7.9	6.6	14.7	18.7	25.6	40.9



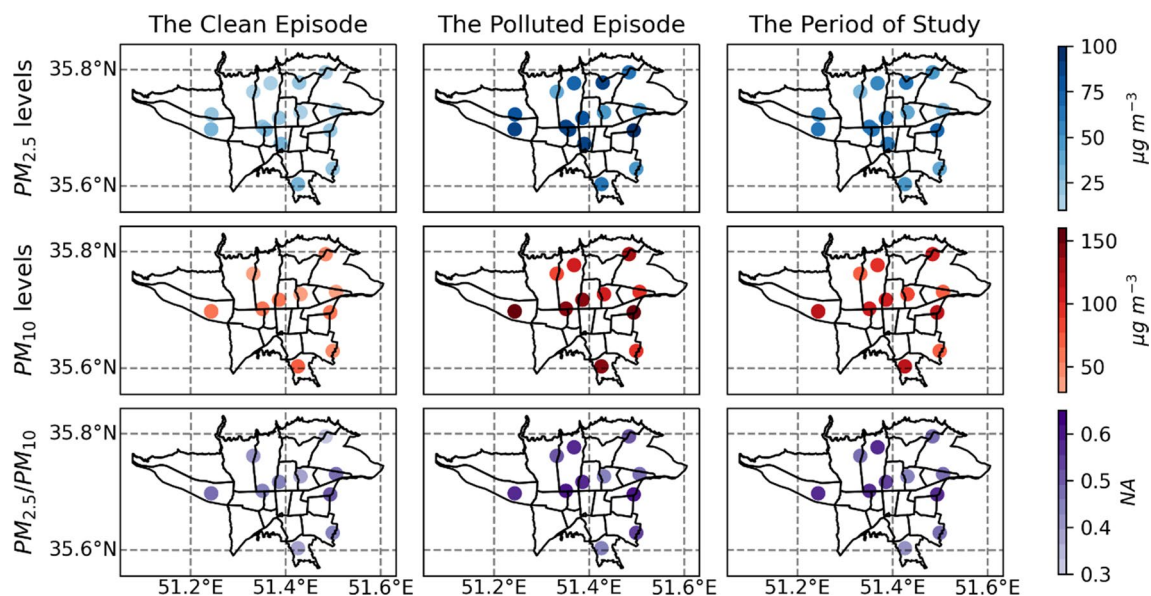


**Fig. 11** Spatial pattern of averaged  $PM_{2.5}$  (top row),  $PM_{10}$  (middle row), and the ratio of  $PM_{2.5}$  to  $PM_{10}$  (bottom row) in the clean episode (left column), the polluted episode (middle column), and the period of study (right column)

of PBLH, we investigate the causality of reduction in PBLH in polluted episode period by these parameters.

The cloud's presence in the middle of the polluted episode leads to a decrease in temperature and an increase in HFX. As a result of higher HFX, PBLH rose above 200 m, and favorable VC provides suitable conditions for PM dispersion (Fig. 12c, d, e). Further, we linked this pollution discharge to the presence of a low-pressure system for a short time over the northeast of Iran. The presence of a high-pressure system from 25th December 2020 until 13th January 2021 accounted for the polluted episode, while a low-pressure system from 14th January 2021 until 21st January 2021 accounted for favorable conditions in the clean episode, as shown in Fig. 12f. In Fig. 12f, these periods are separated by brown and green dashed lines, respectively.

Although the first two days of the high-pressure system resulted in the accumulation of PM levels in the city, PM levels did not reach the harmful range. Even though the low-pressure system replaced the high-pressure system in the late polluted episode, two days were still unhealthy AQI range, as shown in Fig. 12a–f. Moreover, the polluted episode experienced a mean average SLP of 1024.8 hPa. However, the mean average SLP of the clean episode was 1018.8 hPa. It should be noted that the polluted and clean episodes both had high- and low-pressure systems due to the delay in the accumulation and discharge of pollutants at the beginning of the high-pressure system and the beginning of the low-pressure one, respectively.

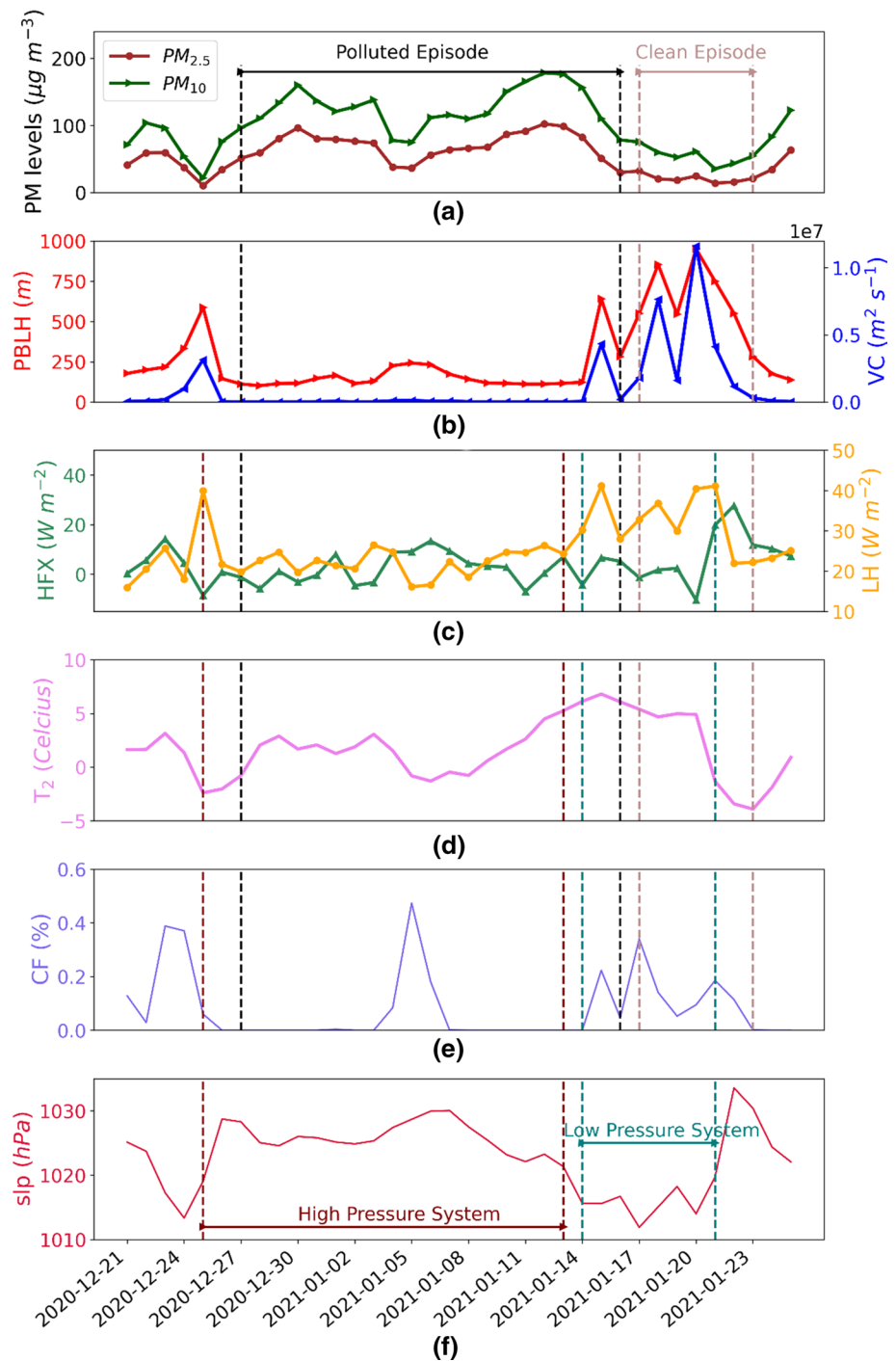
We, in Fig. 13, depict the three columns from the left as a presentation of the high-pressure system and two columns

from the right as a presentation of the low-pressure system. As shown in Fig. 13, the urban areas experienced warmer temperatures during the high-pressure system than the rural area. High HFX correspond with higher PBLH, and as a result, higher VC occurred in the city. On the south of the northern mountains in the plain area, sea level pressure was higher than the high altitudes of mountains. Similar to 2021-01-09, the south and west-south of the city experience higher VC than other parts of the city during the most high-pressure system. Also, the wind direction was toward the city. The wind direction and speed can bring the outside produced pollutants to the city. During the low-pressure system, the temperature is distributed evenly in both rural and urban areas. Higher PBLH in this system happened compared to those in the high-pressure system. Most of the time, the south and west-south of the city had much higher VC than other parts of the city. In the part of the city where the cloud was present, VC decreased compared to cloudless parts of the city.

In comparison, the polluted episode was warmer than the clean episode. Both HFX and LH were higher in the clean episode than the polluted episode. Statistical analysis of sensible heat flux, latent heat flux, temperature, cloud fraction, and sea level pressure are presented in Table 4.

We investigated more in the formation of low- and high-pressure systems in the first domain at 500 mb pressure level, as shown in Fig. 14. Prior to the polluted episode, a low-pressure system across from the northwest of the domain toward the east. Afterward, a high-pressure system from the west with low wind speeds dominated Iran for several days.

**Fig. 12** **a** Daily averaged  $PM_{10}$  and  $PM_{2.5}$  levels from stationary measurements. Daily average of **b** PBLH and VC, **c** sensible heat flux and latent heat flux, **d** air temperature, **e** cloud fraction, and **f** sea level pressure from the WRF model within Tehran boundaries throughout the study period

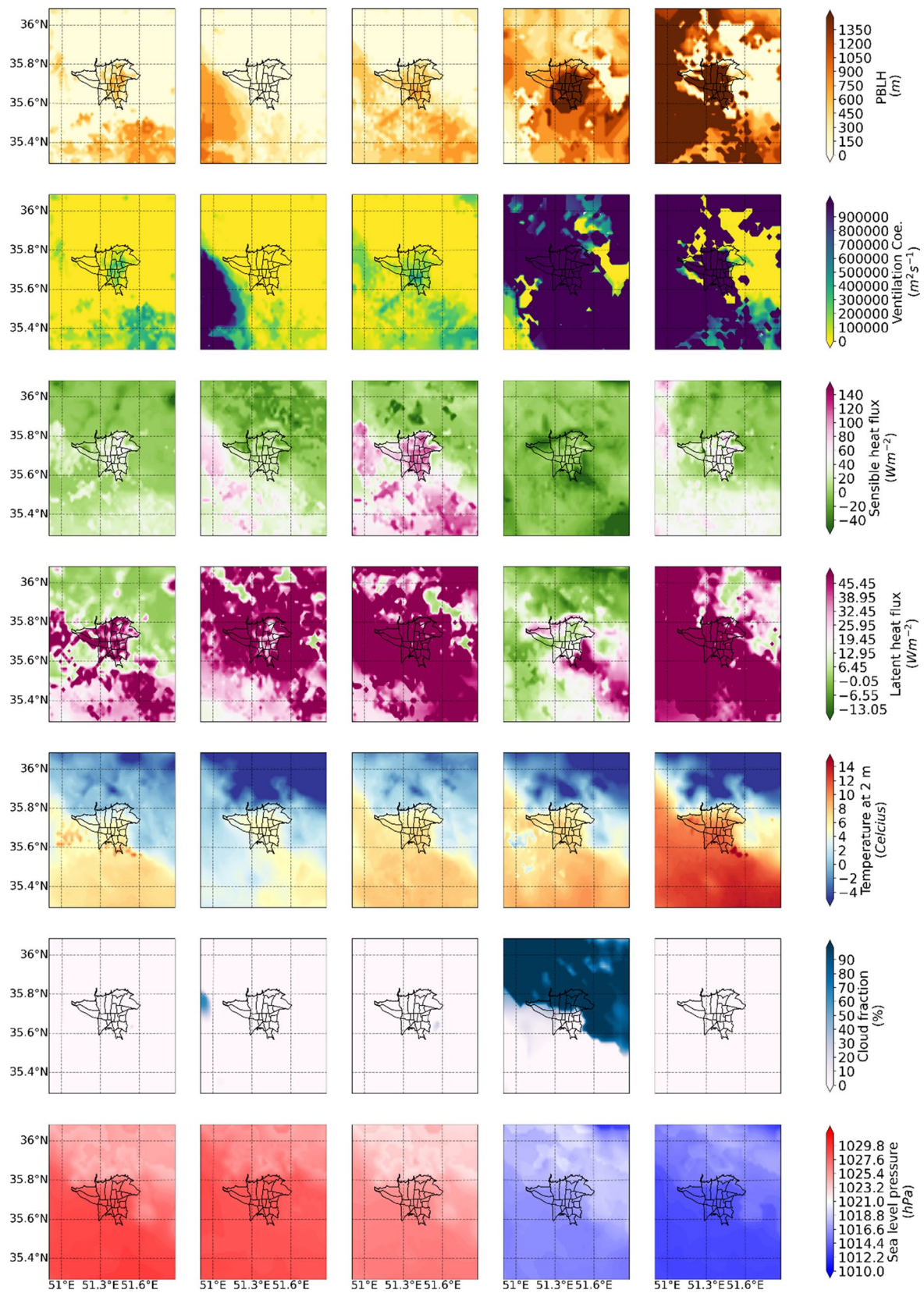


In the middle of the polluted episode (Fig. 14, 2021-01-06), a slight low-pressure with high wind speed across from the north of the domain toward the east. Afterward, the high-pressure system was dominant again. A low-pressure system with high wind speed was the key feature of the clean episode.

## 4 Discussion

### 4.1 Model's uncertainties

We configured WRF-UCM over Tehran to simulate PBLH and VC. Validations of the model showed reasonable performance. The  $T_2$  uncertainties were found to be higher in urban areas compared to rural areas. However, the model



2020-12-27\_12:00 2021-01-04\_06:00 2021-01-09\_10:00 2021-01-15\_16:00 2021-01-20\_12:00



**Fig. 13** Spatial patterns of different parameters captured by the model. (from the top row to bottom) PBLH, VC, sensible heat flux, latent heat flux,  $T_2$ , cloud fraction, sea level pressure, respectively; From left, the first, second, and third columns represent the high-pressure system with the time of 2020-12-27\_12:00, 2021-01-04\_06:00, and 2021-01-09\_10:00, respectively. From left, fourth and fifth columns represent the low-pressure system with the time of 2021-01-15\_16:00 and 2021-01-20\_12:00, respectively

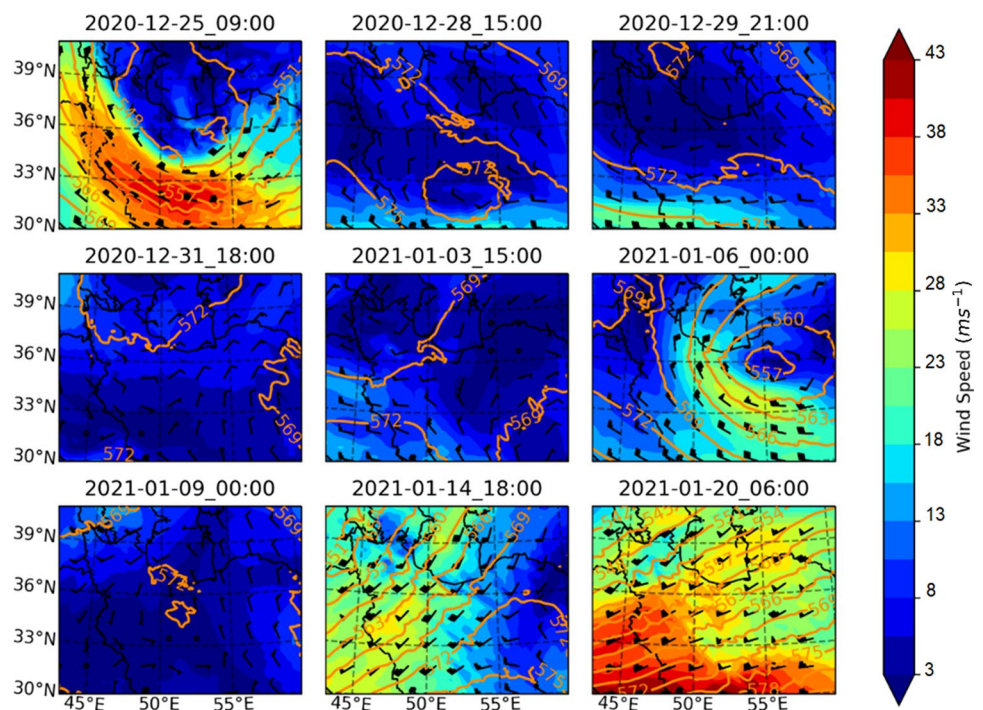
used in this study was able to accurately capture the overall land surface temperature. Salamanca et al. (2018) discussed that while the WRF-UCM model performed well in simulating summertime temperatures (due to calibration to represent the urban heat islands during summer time), it had limitations in capturing wintertime temperatures (in the case of this study in December and January) which were not well represented in the model. On the other hand, Lin et al. (2016) found that the WRF-UCM2D model performed better than the WRF-UCM model, and both studies showed that the Noah-MP surface layer parameterization led to improved wind and temperature performance. Both the Noah and Noah-MP models were able to accurately capture the skin surface temperature. Molnár et al. (2019) showed that based on the defined LCZ in the model, the model’s performance varies from cell to cell. This means the accuracy of the training dataset can affect the model’s performance. According to the Izadi (2021) dataset, the cell associated with Mehrabad station has the industrial/commercial urban type with higher anthropogenic heat. Therefore, the model’s overestimation in  $T_2$  can be expected since the land use type is not correctly trained in that specific urban area.

Furthermore, the model calculated the minimum PBLH (mainly happening during the night) about 50 m which is unrealistic. As Lopez-Coto et al. (2020) reported, most physic parameterization configurations underestimate the PBLH during the night. Therefore, the PBLH during the night needs a better representation. In the case of this study, nighttime PBLH and VC are underestimated by the model. There were some uncertainties in the UCM parameterization and urban-type that we used due to the number of samples and the training accuracy. A more accurate and well-trained dataset could improve the performance of the model. Also, we used default urban surfaces albedo and anthropogenic heat. It should be noted that the WRF-BEP model is mainly used and calibrated over the summertime (Ribeiro et al. 2021; Molnár et al. 2019).

### 4.2 Impact of climate change and meteorology conditions on air pollution

Typical high VCs in the southwest of the city have significant potential to transport local and abroad pollution sources to the inner city. The wind field was also in favor of transporting the non-local pollutants to the city. Therefore, with the advent of a stable high-pressure system, the PBLH and VC will decrease dramatically. This decline is in favor of accumulation and high PM concentrations in the south and southwest. Also, PM levels will increase due to the wind field of the city. On the other hand, high wind speed during the clean episode could contribute to the dust emission (Chen et al. 2021; Csavina et al. 2014; Kurosaki and Mikami

**Fig. 14** Geopotential height (orange contour line), wind speed, and direction (barbs and color contour) at 500 mb of the first domain at different times



2007). However, as Fu et al. (2017) have shown, narrow streets with high buildings along heavy traffics could accentuate the PM levels in the city.

Some studies in other parts of the world showed that the increase in air pollution levels might be the effect of climate change due to changes in the pattern of cyclones and natural ventilation mechanisms (Mickley et al. 2004). Since one of the consequences of change in the pattern and extremes of weather parameters such as PBLH, VC, temperature, etc., could result from climate change, severe air pollution episodes will be expected under the same emission rate in the future. However, more studies are required to determine if this persistent high-pressure system resulted from climate change.

Furthermore, extreme dryness in recent years (Ashraf et al. 2021) led to unstable soil as a result of groundwater depletion, more soil erosion, and dust storms with local sources (Ebrahimi Khusfi et al. 2020) will be expected to happen. They will be brought to the city by high potential VC in the southwest of the city, since the gap of  $PM_{10}$  and  $PM_{2.5}$  have increased in the period of the polluted episode. As higher temperature results in lower  $PM_{2.5}/PM_{10}$ , warmer days of the modeling periods showed a positive correlation with lower  $PM_{2.5}/PM_{10}$ , where traffic emissions contributed to air pollution with a higher  $PM_{2.5}/PM_{10}$  ratio in the cold days of modeling episodes (Xu et al. 2017; Puxbaum et al. 2004). Therefore, resilience in climate change is seemed to have an essential role in air pollution management (Bidokhti et al. 2016; McCollum et al. 2013; Dulal 2017). Since December and January have the lowest PBLH and VC among other months, the necessity of more control and managing over emissions of pollutions become more evident in these months.

## 5 Conclusion

In this study, we set up the WRF-UCM model to investigate the impact of meteorology on the severe episode of air pollution episode in Tehran from 30th December 2020 to 15th January 2021, which resulted in fourteen days with an AQI over 150 (unhealthy). To improve the representation of urban areas in our study, we utilized the available LCZ dataset for Tehran and extracted urban features. The developed methodology using the extracted urban features showed acceptable performance in providing meteorological conditions using the WRF-UCM model. This approach is particularly useful for future studies, as the default settings of the WRF model do not include urban fraction or urban types as input, particularly for Tehran. By incorporating this information, our methodology provides a more accurate representation of urban areas and their impact on meteorology, which in turn can improve our understanding and prediction of air pollution episodes in urban environments.

During the modeling period, the WRF-UCM model demonstrated acceptable performance in capturing 2 m temperature and humidity, as well as 10 m wind speed. Additionally, the model accurately captured land surface temperature in agreement with the satellite observation. However, the model needs improvement in presenting winter temperatures since it is primarily calibrated for summer temperatures. Furthermore, the model underestimates nighttime Planetary Boundary Layer Height (PBLH) and requires better representation.

The low PBLH and VC values in the polluted episode period highly impacted the concentrations of  $PM_{2.5}$  and  $PM_{10}$  in the city. High stable meteorological conditions and a long-lasting high-pressure system intensified the air pollution levels in the urban area of Tehran. The low PBLH and VC result in the accumulation of high concentration in the city, given the complex terrain of the urban area. Notably, this accumulation is highly correlated to wind speed reduction due to an increase in surface roughness as a result of urbanization.

It was observed that pollutants took almost two days to accumulate, resulting in AQI levels higher than moderate during the polluted episode. Similarly, during the clean episode, it took two days for pollutants to be removed by the low-pressure system. Furthermore, non-local pollutants, whether anthropogenic or dust, could significantly impact air pollution in Tehran.

In summary, our study provides valuable insights into the impact of meteorology on air pollution in Tehran. Our methodology provides a useful tool for future research. However, improvements to the model are necessary, particularly in representing winter temperatures and nighttime PBLHs, to enhance the accuracy of the results.

**Acknowledgements** There was no conflict of interest. The authors thank Dr. Niksokhan and Mr. Roozitalab from the Computing Center at the Graduate Faculty of Environment for providing hardware facilities for this research work. All MODIS data products used in this investigation are obtained using EARTHDATA (<https://earthdata.nasa.gov>). All upper-air data were obtained from Wyoming University (<http://weather.uwyo.edu/upperair/sounding.html>). Also, we appreciate the AQCC for the availability of the pollution measurements datasets. It should be noted that significant parts of the visualization and analysis of the simulation's results have been done using python code. This research did not receive any specific grant from the public, commercial, or not-for-profit funding agencies.

**Data availability** Not applicable.

## References

- AQCC. 2021. "Tehran air quality data." Air quality control company of Tehran. 2021. <http://airnow.tehran.ir/home/DataArchive.aspx>. Accessed 10 June 2021

- Arghavani S, Malakooti H, Bidokhti AA (2019) Numerical evaluation of urban green space scenarios effects on gaseous air pollutants in Tehran metropolis based on WRF-chem model. *Atmos Environ* 214:116832. <https://doi.org/10.1016/j.atmosenv.2019.116832>
- Arhami M, Hosseini V, Zare Shahne M, Bigdeli M, Lai A, Schauer JJ (2017) Seasonal trends, chemical speciation and source apportionment of fine PM in Tehran. *Atmos Environ* 153:70–82. <https://doi.org/10.1016/j.atmosenv.2016.12.046>
- Ashrafi K (2012) Determining of spatial distribution patterns and temporal trends of an air pollutant using proper orthogonal decomposition basis functions. *Atmos Environ* 47:468–476. <https://doi.org/10.1016/j.atmosenv.2011.10.016>
- Ashrafi K, Shafiepour Motlagh M, Kamalan H (2009) Estimating temporal and seasonal variation of ventilation coefficients. *Int J Environ Res* 3(4):637–644
- Ashrafi K, Shafiepour Motlagh M, Esmaeili Neyestani S (2017) Dust storms modeling and their impacts on air quality and radiation budget over Iran using WRF-chem. *Air Qual Atmos Health* 10(9):1059–1076. <https://doi.org/10.1007/s11869-017-0494-8>
- Ashraf S, Nazemi A, AghaKouchak A. (2021) “Anthropogenic drought dominates groundwater depletion in Iran.” *Sci Rep* 11(1):9135. <https://doi.org/10.1038/s41598-021-88522-y>.
- Bayat R, Ashrafi K, Shafiepour Motlagh M, Hassanvand MS, Daroudi R, Fink G, Künzli N (2019) Health impact and related cost of ambient air pollution in Tehran. *Environ Res*. <https://doi.org/10.1016/j.envres.2019.108547>
- Bidokhti AA, Shariepour Z, Sehatkashani S (2016) Some resilient aspects of urban areas to air pollution and climate change, case study: Tehran, Iran. *Sci Iran Trans A Civ Eng*. 23(5):1994
- Chen S-H, Sun W-Y (2002) A one-dimensional time dependent cloud model. *J Meteorol Soc Jpn. Ser. II* 80(1):99–118
- Chen F, Kusaka H, Bornstein R, Ching J, Grimmond CSB, Grossman-Clarke S, Loridan T (2011) The integrated WRF/urban modeling system: development, evaluation, and applications to urban environmental problems. *Int J Climatol* 31(2):273–288. <https://doi.org/10.1002/joc.2158>
- Chen S-H, McDowell B, Huang C-C, Nathan TR (2021) Formation of a low-level barrier jet and its modulation by dust radiative forcing over the hexi corridor in central China on 17th March, 2010. *Quart J R Meteorol Soc* 147(736):1873–1891. <https://doi.org/10.1002/qj.4000>
- Cheremisnoff NP (2002) Handbook of air pollution prevention and control. Elsevier, New York
- Chou MD, Suarez MJ (1999) A shortwave radiation parameterization for atmospheric studies. NASA Tech Memo 15(104606):40
- Csavina J, Field J, Félix O, Corral-Avitia AY, Eduardo Sáez A, Berterton EA (2014) Effect of wind speed and relative humidity on atmospheric dust concentrations in semi-arid climates. *Sci Total Environ* 487:82–90
- Demuzere M, Argüeso D, Zonato A, Kittner J (2021) W2W: a python package that injects WUDAPT’s local climate zone information in WRF. *J Open Source Softw*. 7(76):4432
- Du C, Liu S, Yu X, Li X, Chen C, Peng Y, Dong Y, Dong Z, Wang F (2013) Urban boundary layer height characteristics and relationship with particulate matter mass concentrations in Xi’an, Central China. *Aerosol Air Qual Res* 13(5):1598–1607. <https://doi.org/10.4209/aaqr.2012.10.0274>
- Dulal HB (2017) Making cities resilient to climate change: identifying ‘Win–Win’ interventions. *Local Environ* 22(1):106–125
- Ebrahimi Khusfi Z, Khosroshahi M, Roustaei F, Mirakbari M (2020) Spatial and seasonal variations of sand-dust events and their relation to atmospheric conditions and vegetation cover in Semi-Arid Regions of Central Iran. *Geoderma* 365:114225. <https://doi.org/10.1016/j.geoderma.2020.114225>
- EPA. 2018. “Particulate matter (PM) basics|particulate matter (PM) pollution.” 2018. <https://www.epa.gov/pm-pollution/particulate-matter-pm-basics>. Accessed 20 May 2020
- EPA . 2021. “Air Data Basic Information.” Environmental Protection Agency. 2021. <https://www.epa.gov/outdoor-air-quality-data/air-data-basic-information>. Accessed 18 Jan 2021
- Epstein SA, Lee S-M, Katzenstein AS, Carreras-Sospedra M, Zhang X, Farina SC, Vahmani P, Fine PM, Ban-Weiss GA (2017) Air-of quality Implications widespread adoption of cool roofs on ozone and particulate matter in Southern California. *Proc Natl Acad Sci* 114(34):8991–8996. <https://doi.org/10.1073/pnas.1703560114>
- Farahani VJ, Arhami M (2020) Contribution of Iraqi and Syrian dust storms on particulate matter concentration during a dust storm episode in receptor cities: case study of Tehran. *Atmos Environ* 222:117163. <https://doi.org/10.1016/j.atmosenv.2019.117163>
- Fu X, Liu J, Ban-Weiss GA, Zhang J, Huang X, Ouyang B, Popoola O, Tao S (2017) Effects of Canyon geometry on the distribution of traffic-related air pollution in a large urban area: implications of a multi-Canyon air pollution dispersion model. *Atmos Environ* 165:111–121. <https://doi.org/10.1016/j.atmosenv.2017.06.031>
- He G, Pan Y, Tanaka T (2020) The short-term impacts of COVID-19 lockdown on urban air pollution in China. *Nat Sustain* 3(12):1005–1011. <https://doi.org/10.1038/s41893-020-0581-y>
- Heger, M., and Sarraf, M. 2018. “Air Pollution in Tehran: Health Costs, Sources, and Policies.” World Health Organization, no. April: 38. <https://openknowledge.worldbank.org/bitstream/handle/10986/29909/126402-NWP-PUBLIC-Tehran-WEB-updated.pdf?sequence=1&isAllowed=y>. Accessed 28 June 2020
- Iowa Environmental Mesonet. 2021. “IEM: Download ASOS/AWOS/METAR Data.” Iowa State University . 2021. [https://mesonet.agron.iastate.edu/request/download.phtml?network=IR\\_\\_ASOS](https://mesonet.agron.iastate.edu/request/download.phtml?network=IR__ASOS). Accessed 10 June 2020
- Iyer US, Raj PE (2013) Ventilation coefficient trends in the recent decades over four major Indian metropolitan cities. *J Earth Syst Sci* 122(2):537–549. <https://doi.org/10.1007/s12040-013-0270-6>
- Izadi, N. 2021. “WUDAPT Level 0 Training Data for Tehran Mega City (Iran, Islamic Republic of), Submitted to the LCZ Generator.”
- Janjić ZI (1994) The step-mountain Eta coordinate model: further developments of the convection, viscous sublayer, and turbulence closure schemes. *Mon Weather Rev* 122(5):927–945
- Kain JS (2004) The Kain-Fritsch convective parameterization: an update. *J Appl Meteorol* 43(1):170–181. [https://doi.org/10.1175/1520-0450\(2004\)043%3c0170:TKCPAU%3e2.0.CO;2](https://doi.org/10.1175/1520-0450(2004)043%3c0170:TKCPAU%3e2.0.CO;2)
- Krishnan P, Kunhikrishnan PK (2004) Temporal variations of ventilation coefficient at a tropical Indian station using UHF wind profiler. *Curr Sci* 86(3):447–451
- Kurosaki Y, Mikami M (2007) Threshold wind speed for dust emission in East Asia and its seasonal variations. *J Geophys Res Atmos*. <https://doi.org/10.1029/2006JD007988>
- Kusaka H, Kimura F (2004) Thermal effects of urban Canyon structure on the Nocturnal heat island: numerical experiment using a mesoscale model coupled with an urban Canopy model. *J Appl Meteorol* 43(12):1899–1910
- Lin C-Y, Su C-J, Kusaka H, Akimoto Y, Sheng Y-F, Huang J-C, Hsu H-H (2016) Impact of an improved WRF Urban canopy model on diurnal air temperature simulation over Northern Taiwan. *Atmos Chem Phys* 16(3):1809–1822. <https://doi.org/10.5194/acp-16-1809-2016>
- Lopez-Coto I, Hicks M, Karion A, Sakai RK, Demoz B, Prasad K, Whetstone J (2020) Assessment of planetary boundary layer parameterizations and Urban Heat Island comparison: impacts and implications for tracer transport. *J Appl Meteorol Climatol* 59(10):1637–1653. <https://doi.org/10.1175/JAMC-D-19-0168.1>
- Mahalakshmi DV, Badarinath KVS, Naidu CV (2011) “Influence of boundary layer dynamics on pollutant concentrations over urban



- region—a study using ground based measurements.” *Indian J Radio Space Phy* 40:147–152.
- McCollum DL, Krey V, Riahi K, Kolp P, Grubler A, Makowski M, Nakicenovic N (2013) Climate policies can help resolve energy security and air pollution challenges. *Clim Change* 119(2):479–494
- Mickley LJ, Jacob DJ, Field BD, Rind D (2004) Effects of future climate change on regional air pollution episodes in the United States. *Geophys Res Lett*. <https://doi.org/10.1029/2004GL021216>
- Mlawer EJ, Taubman SJ, Brown PD, Iacono MJ, Clough SA (1997) Radiative transfer for inhomogeneous atmospheres: RRTM, a validated correlated-k model for the longwave. *J Geophys Res Atmos* 102(D14):16663–16682
- Molnár G, Gyöngyösi AZ, Gál T (2019) Integration of an LCZ-based classification into WRF to assess the intra-urban temperature pattern under a heatwave period in Szeged, Hungary. *Theoret Appl Climatol* 138(1):1139–1158. <https://doi.org/10.1007/s00704-019-02881-1>
- Niu G-Y, Yang Z-L, Mitchell KE, Chen F, Ek MB, Barlage M, Kumar A, Manning K, Niyogi D, Rosero E (2011) The community Noah land surface model with multiparameterization options (Noah-MP): 1. Model description and evaluation with local-scale measurements. *J Geophys Res Atmos*. <https://doi.org/10.1029/2010JD015139>
- Pishgar E, Fanni Z, Tavakkolinia J, Mohammadi A, Kiani B, Bergquist R (2020) Mortality rates due to respiratory tract diseases in Tehran, Iran during 2008–2018: a spatiotemporal, cross-sectional study. *BMC Public Health* 20(1):1414. <https://doi.org/10.1186/s12889-020-09495-7>
- Puxbaum H, Gomiscek B, Kalina M, Bauer H, Salam A, Stopper S, Preining O, Hauck H (2004) A dual site study of PM<sub>2.5</sub> and PM<sub>10</sub> aerosol chemistry in the larger region of Vienna, Austria. *Atmos Environ* 38(24):3949–3958. <https://doi.org/10.1016/j.atmosenv.2003.12.043>
- Ribeiro I, Martilli A, Falls M, Zonato A, Villalba G (2021) Highly resolved WRF-BEP/BEM simulations over Barcelona urban area with LCZ. *Atmos Res* 248:105220. <https://doi.org/10.1016/j.atmosres.2020.105220>
- Salamanca F, Zhang Y, Barlage M, Chen F, Mahalov A, Miao S (2018) Evaluation of the WRF-urban modeling system coupled to Noah and Noah-MP land surface models over a Semiarid urban environment. *J Geophys Res Atmos*. 123(5):2387–2408. <https://doi.org/10.1002/2018JD028377>
- Shahbazi H, Reyhanian M, Hosseini V, Afshin H (2016) The relative contributions of mobile sources to air pollutant emissions in Tehran, Iran: an emission inventory approach. *Emiss Control Sci Technol* 2(1):44–56. <https://doi.org/10.1007/s40825-015-0031-x>
- Skamarock WC, Klemp JB, Dudhia J, Gill DO, Barker DM, Duda MG, Huang X-Y, Wang W, Powers JG (2019) “A description of the advanced research WRF Version 4”, Mesoscale and Microscale Meteorology Division, National Center for Atmospheric Research (NCAR), NCAR TECHNICAL NOTES, <https://doi.org/10.6084/M9.FIGSHARE.7369994.V4>
- Statistical Center of Iran. 2016. “Selected Findings of the 2016 National Population and Housing Census.” [https://www.amar.org.ir/Portals/1/census/2016/Census\\_2016\\_Selected\\_Findings.pdf](https://www.amar.org.ir/Portals/1/census/2016/Census_2016_Selected_Findings.pdf). Accessed 10 Jan 2022
- Statistical Center of Iran. 2021. “Climate and Environment.” Statistics by Topic. 2021. <https://www.amar.org.ir/english/Statistics-by-Topic/Climate-and-Environment>. Accessed 10 Jan 2022
- Su T, Li Z, Zheng Y, Luan Q, Guo J (2020) Abnormally shallow boundary layer associated with severe air pollution during the COVID-19 lockdown in China. *Geophys Res Lett* 47(20):e2020GL090041. <https://doi.org/10.1029/2020GL090041>
- Sujatha P, Mahalakshmi DV, Ramiz A, Rao PVN, Naidu CV (2016) Ventilation coefficient and boundary layer height impact on urban air quality. *Cogent Environ Sci*. <https://doi.org/10.1080/23311843.2015.1125284>
- Vahmani P, Ban-Weiss GA (2016) Impact of remotely sensed albedo and vegetation fraction on simulation of urban climate in WRF-urban Canopy model: a case study of the urban heat island in Los Angeles. *J. Geophys. Res. Atmos* 121:1511–1531. <https://doi.org/10.1002/2015JD023718>
- Vahmani P, Sun F, Hall A, Ban-Weiss GA (2016) Investigating the climate impacts of urbanization and the potential for cool roofs to counter future climate change in Southern California. *Environ Res Lett* 11(12):124027. <https://doi.org/10.1088/1748-9326/11/12/124027>
- Wang W, Bruyère C, Duda M, Dudhia J, Gill D, Kavulich M, Werner K (2018) “Advanced research WRF (ARW) Version 4.0 modeling system user’s guide,” no. June: 464.
- World Bank. 2020. “Pollution.” World Bank. 2020. <https://www.worldbank.org/en/topic/pollution>. Accessed 10 Jan 2022
- Xu G, Jiao L, Zhang B, Zhao S, Yuan M, Gu Y, Liu J, Tang X (2017) Spatial and temporal variability of the PM<sub>2.5</sub>/PM<sub>10</sub> ratio in Wuhan, Central China. *Aerosol Air Qual Res* 17(3):741–751. <https://doi.org/10.4209/aaqr.2016.09.0406>
- Yousefian F, Faridi S, Azimi F, Aghaei M, Shamsipour M, Yaghmaeian K, Hassanvand MS (2020) Temporal variations of ambient air pollutants and meteorological influences on their concentrations in Tehran during 2012–2017. *Sci Rep* 10(1):1–11. <https://doi.org/10.1038/s41598-019-56578-6>

**Publisher's Note** Springer Nature remains neutral with regard to jurisdictional claims in published maps and institutional affiliations.

Springer Nature or its licensor (e.g. a society or other partner) holds exclusive rights to this article under a publishing agreement with the author(s) or other rightsholder(s); author self-archiving of the accepted manuscript version of this article is solely governed by the terms of such publishing agreement and applicable law.